9 Principles of Josephson-Junction-Based Quantum Computation

S. E. Shafranjuk Department of Physics and Astronomy, Northwestern University, Evanston, IL 60208, USA
J. B. Ketterson Department of Physics and Astronomy, Northwestern University, Evanston, IL 60208, USA

9.1 Introduction

One of several approaches that have been proposed for implementing quantum information processing is to utilize mesoscopic, artificially fabricated, solid-state structures which, based on the underlying physics, can be designed to behave as single "quantum particles." The primary reason for a solid state approach is that it offers the likelihood of scalability by exploiting fabrication strategies made possible by the semiconductor industry; scalability is essential if quantum information processing is to become a practical reality. Aside from practical applications, the study of such mesoscopic structures is of interest in its own right.

Quantum information processing is typically based on an assembly of quantum bit devices, so-called *qubits* [1], a term the community has adopted. Such devices involve externally controlled transitions between two quantum states, $|0\rangle$ and $|1\rangle$, corresponding to two different eigenenergies, E_0 and E_1. There are now many proposals for qubits involving various two-level systems. However such elementary quantum logic devices must satisfy strict requirements if they are to be used as quantum logic elements in realistic information processing circuits. A practical circuit utilizing qubits must permit: (*i*) controlled manipulations of the quantum state of each qubit *without disturbing adjacent elements* and (*ii*) controlled inter-qubit coupling; also required are (*iii*) a limited influence of the external environment and (*iv*) sufficiently long dephasing and decoherence times [2,3]. If these requirements cannot be fulfilled, reliable qubit circuits cannot be realized, which currently eliminates many qubit proposals.

Quantum computation (QC) employs and requires a programmable unitary evolution of the individual qubits [4]. Because the proposed systems exploit quantum parallelism and quantum algorithms, they are capable of efficiently solving certain classes of problems, which are intractable on classical computers. A striking example is the factorizing of large numbers [5], which is far more efficient on a quantum computer than on a conventional one.

Along with the development of the theory of quantum information, there has been a parallel interest in finding physical systems where quantum computation can be implemented. Toward this end, one must first identify a suitable two-level system, which is sufficiently decoupled from any source of decoherence [6], and for which the coupling among like elements can be controlled, thereby allowing the realization of single- and two-qubit operations. In principle one can then carry out any computational task if requirements (i)–(iv) are fulfilled [2,3,7]

For the implementation of quantum algorithms various physical systems have been suggested. Some of these proposals involve: ions in traps, [8] QED cavities, [9] and NMR-based approaches [10]. To achieve large-scale integrability and flexibility in the design, approaches involving micro- or even nanotechnology are being examined including: small-capacitance Josephson junctions [11–15], coupled quantum dots [16, 17], neutral atoms in optical lattices [18], and phosphorus dopants in silicon crystals1 [19]. Most of the solid-state based efforts concentrate on superconducting qubits, specifically Josephson junction based qubits [3], and we will review recent junction-based experiments and their theoretical interpretation. The experimental evidence for the superposition of charge states in Josephson junctions [20,21] and recent achievements in controlling the coherent evolution of quantum states in a "Cooper pair box" [22] make superconducting circuits very promising candidates to implement solid state quantum computing.

Figure 9.1 shows a schematic representation of a Josephson junction. Superconducting qubits exploit Cooper pair tunneling between the superfluid condensates in adjacent superconducting electrodes. The Josephson interaction across a dielectric barrier has an intrinsic non-linear origin, which plays an important role in the design of the qubit devices. Josephson junction based qubits, depending on the external configuration, exploit the order-parameter phase, magnetic flux, or electric charge, as shown schematically in Fig. 9.2. Combinations of these configurations are also exploited.

This chapter is organized as follows. In Sect. 9.2 we briefly describe the three Josephson junction based qubit devices, the phase qubit, the charge qubit, and the flux qubit, along with experiments on some spe-

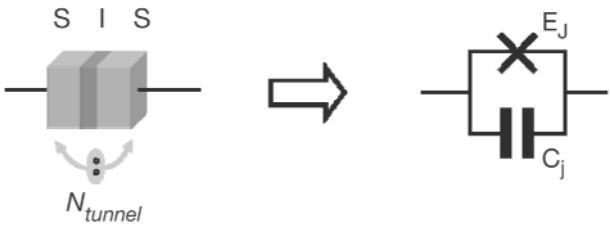

Fig. 9.1. A schematic representation of a Josephson junction and the equivalent circuit

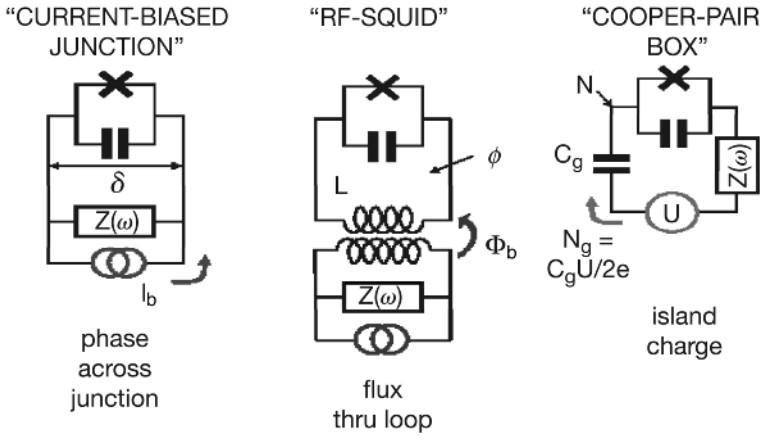

Fig. 9.2. The three major Josephson-junction-based qubit implementations

cific implementations. We also discuss so-called hybrid qubits that combine aspects of both charge and flux qubits.

Section 9.3 starts with a review of the quantum mechanics of two-level systems, which underlies all qubit operations. This is followed by a discussion of the effects of decoherence arising from coupling to external degrees of freedom. It is crucial to maintain the coherence of the two basic qubit states during a quantum computation [2]. The decoherence time, τ_{dec}, of the individual qubits should be larger, by a factor of order 10^4, than a time t_{op}, required to carry out a single operation; one can then carry our arbitrarily long quantum computations by exploiting various error-correction techniques. In solid state implementations, due to the complexity of the environment, there are many degrees of freedom that can couple to the qubit states and cause decoherence. Compared with the photonic and atomic qubit strategies, the superconducting persistent current qubit is subject to more severe decoherence. Dominant sources of decoherence include both "internal" effects, such as *dissipation*, e.g., from quasiparticle resistance, and *dephasing* from qubit interactions with the external environment. These mechanisms depend strongly on the geometry, and on fluctuations of the environment (e.g., nuclear spin fluctuations in aluminum), on background charge noise, and on noise in the control currents. It is also possible to couple to an environmental degree of freedom, without a dissipative mechanism, that will still lead to decoherence. We will outline the general formalism that can be used to deal with the dephasing caused by thermal fluctuations, including quasiparticle dissipation, charge oscillations, nuclear spin relaxation, etc. However we will not, for the most part, try to analyze such mechanisms in detail.

Section 9.3 then goes on to discuss some experiments on single qubit operations that have been carried out on phase and charge qubits. The challenge in performing accurate qubit operations lies in effectively isolating the two energy levels from the rest of Hilbert space. In other words, how does one operate as quickly, and with as little error as possible, on the qubit subspace, while simultaneously isolating the remaining Hilbert space. This is especially

important when the coherence time of the system is short. As an example, a Josephson phase qubit can be described by three energy levels $|0\rangle$, $|1\rangle$, and $|2\rangle$, with energies E_0, E_1, and E_2. The qubit space is formed by $|0\rangle$ and $|1\rangle$, and hence we wish to operate *only* within this subspace. Clearly, the higher-order state can be avoided when working in the $|0\rangle$, $|1\rangle$ sub-space provided the energies differ sufficiently and the excitation pulse is long enough. However, because one wants to maximize the number of logic operations within a fixed coherence time, there is a need to mix the $|0\rangle$ and $|1\rangle$ states as quickly as possible without affecting other states.

Operations on charge qubits can be carried out using the gate voltage alone. However much better control is achieved using a hybrid qubit where the charging and Josephson energies can be individually controlled. Extensive experiments with this device demonstrating controlled decoupling from the external environment are also described.

Section 9.4 describes a two-qubit gate involving two capacitively coupled hybrid qubits and some associated experiments. Section 9.5 discusses a recently proposed and promising two-qubit gate where the qubit coupling is engineered into a single device and which is based on a multilayer SISIS junction.

Finally Sect. 9.6 discusses our conclusions where we examine the outlook for Josephson-junction-based quantum computing.

Although it is not the focus of this article, we briefly outline the elementary quantum logic operations that are necessary for performing quantum computations in Appendix A.

Errors induced by the gate operations themselves must be considered if fault-tolerant quantum computation is to be achieved. The most obvious example is fluctuations in the control parameters of the gate, which act as random noise and thus degrade the unitarity of the time evolution of the computational degrees of freedom. In addition, the actual gate operations can change the qubit coupling to the external environment (even if the coupling is negligible during storage periods) thereby enhancing decoherence.

Most sources of error can be analyzed by properly modeling the qubit-environment coupling. However, there are errors, which are not due to (or cannot be described in terms of) the action of an external environment. An (intrinsic) source of error in gate operations, [23] which is common to several of the proposed solid-state implementations, is so-called *quantum leakage*. It occurs when the computational space is a subspace of a larger Hilbert space. The effects of such states have been investigated for ion trap quantum computers where estimates have been obtained of the number of operations before decay processes induce dissipative transitions outside the computational space [8]. A procedure for estimating the leakage for a phase qubit will be given in Sect. 9.3.2.

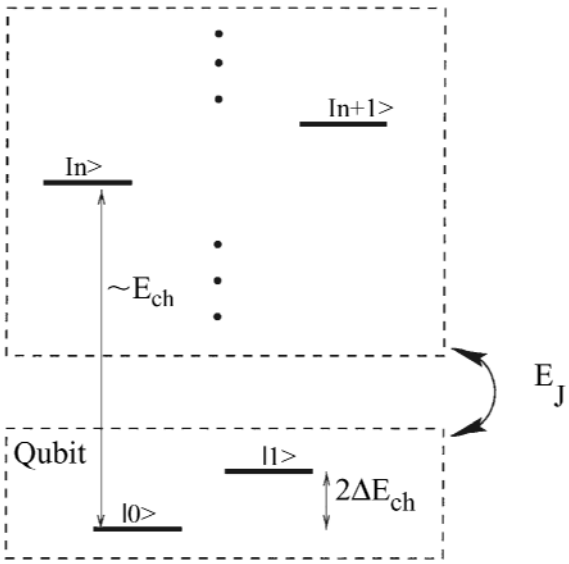

Fig. 9.3. Schematic view of a qubit with leakage (according to [23]). The two low-energy states constitute the computational Hilbert space. The system, however, evolves under the action of some unitary operator and can leak out to the higher excited states. In the case of Josephson junction qubits, leakage is due to the Josephson tunneling to higher charge states. In the case of two-qubit operations, the computational space is spanned by the states $|00\rangle$, $|01\rangle$, $|10\rangle$, $|11\rangle$ and the coupling with the higher charge states is due both to E_J and to inter-qubit coupling E_I. The two low-energy states constitute the computational Hilbert space. However the system can leak out to the higher states. If the energy difference between the low-lying and the excited states is large compared to the other energy scales of the system, the probability to leak out is small

Non-computational states affect the gate dynamics even in the absence of dissipative processes. Such an analysis applies to the situation illustrated schematically in Fig. 9.3; the quantum states $|0\rangle$ and $|1\rangle$ (with the level splitting $\sim 2E_{\rm ch}$, $E_{\rm ch}$ being the charging energy) are affected by the higher excited states $|n\rangle$ and $|n+1\rangle$, which have the same order of level splitting $\sim E_{\rm ch}$ due to Josephson tunneling (associated with an energy $E_{\rm J}$). In two-qubit gates the states also leak due to the inter-qubit coupling which energy is $E_{\rm I}$.

9.2 Josephson-Junction-Based Qubit Devices

In this section we briefly review some approaches to realizing Josephson-junction-based qubits. The flexibility of the Josephson-based circuits allows different implementations, some of which are now being developed by various laboratories.

9.2.1 Junction Parameters and Energetics

Figure 9.4 shows, schematically, a Josephson tunnel junction together with its equivalent circuit. The junction is parameterized by a critical current, I_0, a capacitance, C, and a (in general nonlinear) shunt resistance, R, which here we assume to be large. The superconducting layers are characterized by Landau-Ginzburg order parameters $\psi_i = A_i e^{i\varphi_i}$ with amplitudes, A_1 and A_2, and phases φ_1 and φ_2 of the respective superfluid condensates.

The Josephson coupling energy between the layers depends on the phase difference $\varphi = \varphi_1 - \varphi_2$

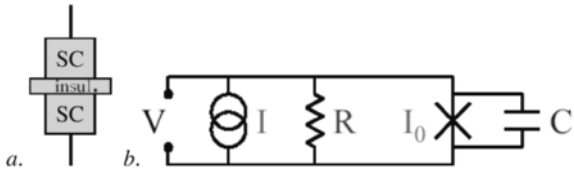

Fig. 9.4. Sketch of the SIS tunneling Josephson junction and its equivalent circuit

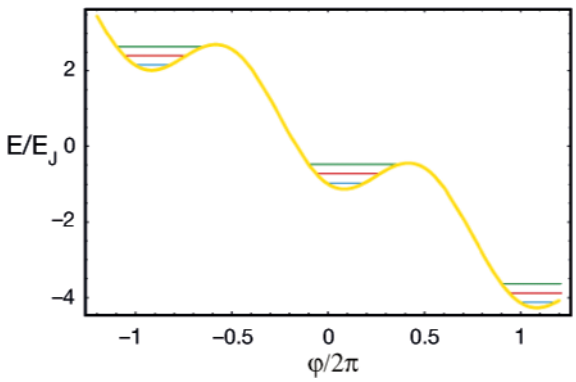

Fig. 9.5. Potential energy (in units of maximal Josephson energy $E_{\rm J}$) of a tunnel junction biased by a supercurrent, I

and plays the role of a "potential energy". We will show shortly that in the presence of an external bias supercurrent this potential energy has the form

$$U(\varphi) = \frac{\Phi_0}{2\pi}\left(I_0 \sin\varphi - \varphi I\right); \qquad (9.1)$$

i.e., it has the shape of a "tilted washboard", as shown in Fig. 9.5. This energy profile is exploited in the large area Josephson junction qubits. Figure 9.6 shows the

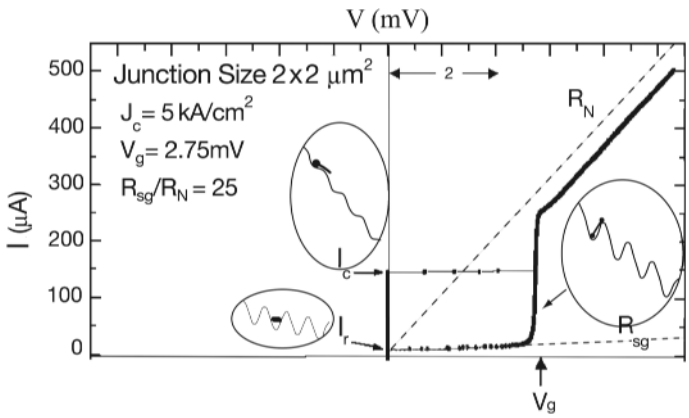

Fig. 9.6. The interior of the ellipses shows the tilting of the "washboard potential" at different positions on the voltage–current characteristic of the Josephson junction. The parameters of the junction (Lukens group, SUNY) are shown in the *inset*

current-voltage characteristic (the I–V curve) of a voltage biased tunnel junction (the parameters being indicated in the inset); also shown is the property that the "washboard" tilt depends on the position on the I-V curve.

When the junction is embedded in a circuit having an external inductance L_s, the behavior depends on its size relative to a characteristic inductance $L_J \equiv \Phi_0/2\pi I_0$ (where $\Phi_0 = h/2e$ is the flux quantum). One then has two limiting cases: $L_s \ll L_J$, in which the induced flux in the loop is unimportant, and $L_s \gg L_J$ where it plays a key role. Circuits of the first type ($L_s \ll L_J$) are usually based on aluminum junctions while circuits of the second type (for which $L_s \gg L_J$) are usually based on niobium. When $L_s \ll L_J$ the properties are determined by the relation between the maximum Josephson coupling energy, $E_J = I_0\Phi_0/2\pi$, and the elementary Coulomb energy, $e^2/2C$.

9.2.2 The Basic Josephson Qubit Categories

We now briefly review some Josephson-junction-based qubits. The flexibility of the Josephson-based circuits allows different implementations, some of which are now being developed by various laboratories. Depending on the variable manipulated, and the junction energetics, we identify the following qubit categories: (*i*) the *phase qubit* with $E_J \gg E_c$ (by a factor 10^3), where the current density j is the variable; (*ii*) the *charge qubit* with $E_J < E_c$, where the charge Q is the variable; and (*iii*) the *flux qubit* with $E_J \gg E_c$ (by a factor 10^2–10^3), where the magnetic flux Φ is the variable. We now give a brief description of each of these three cases.

9.2.3 Phase Qubits

The total current across the junction in Fig. 9.4b is given by

$$I = V/R + I_0 \sin\varphi + C\dot{V} \,. \tag{9.2}$$

Using the Josephson relation, $V = (\hbar/2e)\dot{\varphi}$, and assuming the current I is constant, which allows us to write $I = \partial\phi\,(I\varphi)/\partial\varphi$, we can rewrite Eq. (9.2) as

$$C\left(\frac{\Phi_0}{2\pi}\right)^2 \ddot{\varphi} + \frac{1}{R}\left(\frac{\Phi_0}{2\pi}\right)^2 \dot{\varphi} + \frac{\partial}{\partial\varphi}\left[-I_0\frac{\Phi_0}{2\pi}\cos\varphi - I\frac{\Phi_0}{2\pi}\varphi\right] = 0 \,, \tag{9.3}$$

where $\Phi_0 = h/2e$ is the superconducting flux quantum. The first term in Eq. (9.3) can be associated with a "kinetic energy" K which takes the various forms

$$K = \frac{Q^2}{2C} = \frac{1}{2}CV^2 = \left(\frac{\Phi_0}{2\pi}\right)^2 \dot{\varphi}^2 \,. \tag{9.4}$$

The potential energy of the junction itself is given by

$$U = \int I_J V \mathrm{d}t = \frac{I_0\Phi_0}{2\pi}\int \sin\varphi \frac{d\varphi}{dt}\mathrm{d}t = -\frac{I_0\Phi_0}{2\pi}\cos\varphi \,; \tag{9.5}$$

from this expression it follows that we can interpret Eqs. (9.2) and (9.3) in terms of the motion of a classical particle in a "tilted washboard" potential of the form

$$\tilde{U} = -I_0\frac{\Phi_0}{2\pi}\cos\varphi - I\frac{\Phi_0}{2\pi}\varphi \,; \tag{9.6}$$

this system is shown in Fig. 9.7. Neglecting damping ($R \to \infty$), the potential energies given by Eqs. (9.5) and (9.6) together with the above kinetic energy, $K = q^2/2C$, yield the Hamiltonian under which the classical system evolves in time

$$H(q,\varphi) = K + \tilde{U} = \frac{Q^2}{2C} - \frac{I_0\Phi_0}{2\pi}\cos\varphi - \frac{I\Phi_0}{2\pi}\varphi \,, \tag{9.7}$$

where the charge q plays the role of a momentum, C is a mass, and φ is a coordinate.

We now make the transition to quantum mechanics by writing

$$\hat{H} = \frac{1}{2C}\hat{Q}^2 - \frac{I_0\Phi_0}{2\pi}\cos\varphi - \frac{I\Phi_0}{2\pi}\varphi \,, \tag{9.8}$$

where $\hat{Q} = (2e/i)\partial/\partial\varphi$ and we have the commutation relation $\left[\hat{Q}, \varphi\right] = 2ei$. Quantum mechanical behavior can be observed for large area junctions for which $I_0\Phi_0/2\pi = E_J \gg E_C = e^2/2C$ and when the bias current I is somewhat smaller than the critical current I_0. In this regime the potential $\tilde{U}(\varphi)$

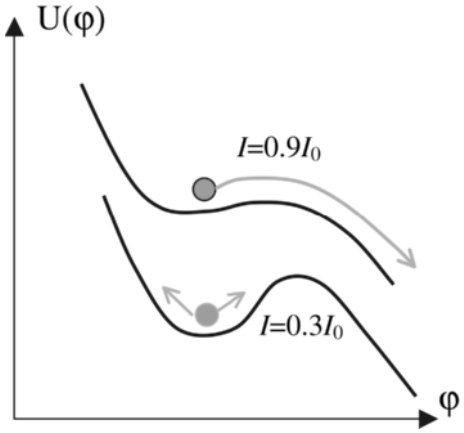

Fig. 9.7. The motion of a classical particle in a "tilted washboard" potential. When the tilt is small (the *lower profile*), the particle oscillates inside the local "washboard" minimum. However at steeper inclines, the particle escapes to an adjacent minimum or, if the damping is small, rolls steadily down the "washboard" (corresponding to as finite voltage state)

can be expanded (about the displaced minimum resulting from the constant current I) and accurately approximated by a cubic polynomial involving a barrier height $\Delta U\,(I) = \left(2\sqrt{2}I_0\Phi_0/3\pi\right)\left[1 - I/I_0\right]^{3/2}$ and a quadratic curvature at the bottom of the well that gives a classical oscillation frequency $\omega_p\,(I) = 2^{1/4}\left(2\pi I_0/\Phi_0 C\right)^{1/2}\left[1 - I/I_0\right]^{1/4}$. The commutation relation leads to quantized energy levels in this cubic potential, which are shown schematically in Fig. 9.8.

When operating the junction as a qubit, one adjusts the tilt to achieve two states lying deeper in the potential well with a third level positioned near the top. The escape rates, Γ_n and Γ_{n+1}, from levels n and $n+1$ to an adjacent well differ significantly from each other; a typical ratio is, $\Gamma_n/\Gamma_{n+1} \sim 10^2$.

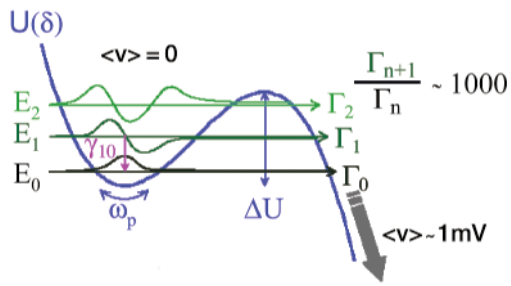

Fig. 9.8. Some quantized states in the quantum well created by the Josephson energy profile

Microwave bias currents induce transitions between levels at a frequency $\omega_{mn} = E_{mn}/\hbar = (E_m - E_n)/\hbar$, where E_n is the energy of state $|n\rangle$. In the cubic approximation the two lowest transitions have the frequencies [24]

$$\omega_{10} \approx \omega_p\left(1 - \frac{5}{36}\frac{\hbar\omega_p}{\Delta U}\right) \tag{9.9}$$

and

$$\omega_{21} \approx \omega_p\left(1 - \frac{10}{36}\frac{\hbar\omega_p}{\Delta U}\right). \tag{9.10}$$

These two frequencies must differ if we are to access the two-state system in a controllable way. The ratio $\Delta U/\hbar\omega_p$ parameterizes the anharmonicity of the cubic potential with regard to the qubit states, and gives an estimate of the number of states in the well. The result of the quantization is to create states inside a local minimum of the washboard, as shown in Fig. 9.8. (Due to tunneling these states are more correctly viewed as resonances with widths Γ_n.) The dependence of ω_{10}, ω_{21}, and ω_{32} on the anharmonicity ratio, $\Delta U/\hbar\omega_p$, is given in Fig. 9.9.

The challenge in performing accurate qubit operations lies in successfully isolating the two lowest energy levels from the rest of the state space; clearly

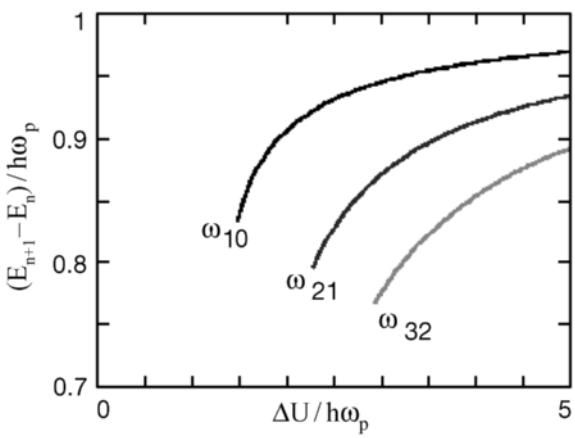

Fig. 9.9. The dependence of the transition frequencies ω_{10}, ω_{21} and ω_{32} between levels on the anharmonicity ratio $\Delta U/\hbar\omega_p$

one wants to operate quickly in the qubit subspace (to minimize the effects of decoherence, see Sect. 9.3.2) with as little coupling to unintended states as possible. This is especially important when the coherence times of the system are short.

A Josephson phase qubit involves three energy levels $|0\rangle$, $|1\rangle$, and $|2\rangle$, with energies E_0, E_1, and E_2. The qubit space is formed by $|0\rangle$ and $|1\rangle$, while the third level is used as a readout (by exploiting its high tunneling rate). The $|0\rangle \leftrightarrow |2\rangle$ transition can be minimized by exciting the $|0\rangle \leftrightarrow |1\rangle$ transition (having a frequency ω_{10}) with a sufficiently long pulse. However, because one wants to maximize the number of logic operations within a fixed coherence time, there is a need to excite the $|0\rangle \leftrightarrow |1\rangle$ transition as quickly as possible without populating other states.

The state of the qubit is determined by a combination of a dc bias current, $I_{\rm dc}$, and a time-varying microwave bias current, $I_{\mu w}(t)$, at a frequency $\omega = \omega_{10}$

$$I(t) = I_{\rm dc} + \Delta I(t) = I_{\rm dc} - I_{\mu w}(t)\cos(\omega t + \phi)\,. \tag{9.11}$$

9.2.4 Charge Qubits

The Single Junction Charge Qubit

We now consider the case $E_C > E_J$ (by a few orders of magnitude); this leads us to a different class of devices, the so-called charge qubits. The simplest example of such a device is shown schematically in Fig. 9.10. It involves two superconducting strips, S_1 and S_2 one of which slightly overlaps the other, but which are separated by an oxide barrier so as to form a Josephson junction; this junction is characterized by a capacitance C_J and critical current I_0 where the latter is associated with a Josephson energy, E_J. One of these strips (designated S_2 in the figure) is called the *island* or *Cooper charge box*; it has a self-capacitance C_I and it is coupled to an adjacent third strip, called the gate, through a capacitance C_G to which a voltage V_G is applied. It is assumed that there is no Josephson coupling between the gate and the island and that the gate can be biased relative to the island by a voltage V_G. A typical island capacitance, C_I, is $\leq 10^{-15}$F, while the gate capacitance is typically smaller.

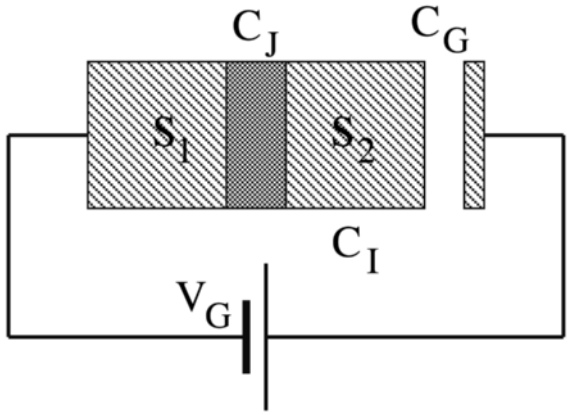

Fig. 9.10. The basic circuit of a single junction charge qubit

It is assumed the device is configured such that the superconducting energy gap, Δ, is the largest energy in the system and hence at low temperatures ($\Delta \gg k_B T$) quasiparticle tunneling can be neglected. Under this circumstance coherent tunneling of Cooper pairs is the only channel between the island and the superconducting electrode and the charge of the island is restricted to $2Ne$ where N, the number of *excess* Cooper pairs, is an integer.

The electrostatic energy associated with devices of this type is somewhat subtle. We will not discuss this problem here but rather refer the reader to an analysis by Tinkham who obtains the form [25]

$$E_{\rm Coulomb} = 4E_C\,(N - N_G)^2 + \text{const.}\,, \tag{9.12}$$

where the constant can be ignored, $E_C \equiv e^2/2C_I$ is the *single electron* charging energy of the island, and N_G is the number of Cooper pairs *induced* electrostatically by the gate on the island; N_G can be written in terms of the gate voltage as $N_G = C_G V_G/2e$. When there are no excess Cooper pairs on the island ($N = 0$) the energy increases quadratically with the gate voltage, as with any capacitor; this behavior is shown by the black parabola in Fig. 9.11. The energy in the presence of a single excess Cooper pair on the island is shown by the red parabola. Note $E_{\rm Coulomb}$ vanishes for $N_G = 1$ or, equivalently, at a gate voltage $V_G = 2e/C_G$. On the other hand, at the point $N_G = 1/2$, where the red and black parabolas in Fig. 9.11 cross each other, two many-body superconducting ground states of the island would be

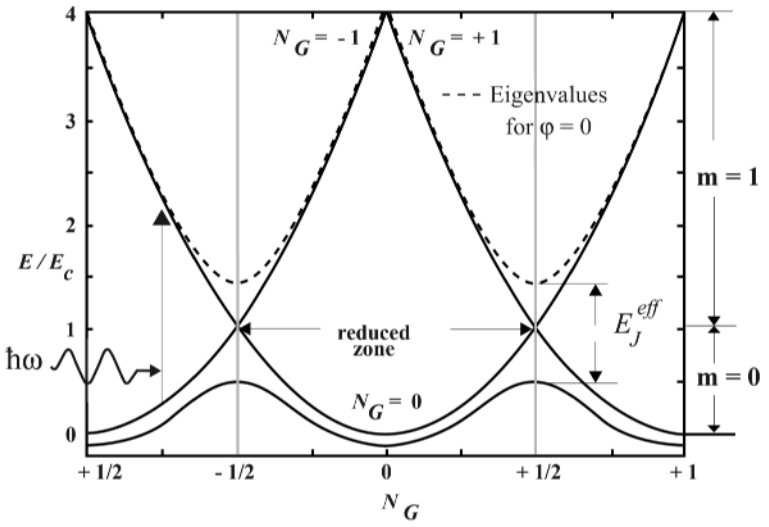

Fig. 9.11. The energy diagram of a charge qubit

degenerate in the absence of the Josephson coupling (which we have been assuming small compared with the Coulomb energy); i.e. the states with that $N = 0$ and $N = 1$ would have the same energy. Hence V_G can be used as a *control parameter* to perform quantum superpositions of these many-body superconducting charge states.[1]

As with the phase qubit discussed above, the dynamics of the device are again governed by a classical Hamiltonian that is the sum of an electrostatic kinetic energy, given by Eq. (9.12), and the Josephson potential energy. To transition to quantum mechanics, in a representation where the Josephson *phase* is diagonal, the electrostatic energy is interpreted as a kinetic energy *operator*, $K = 4E_C(\hat{N} - N_G)^2$; here $\hat{N} = -i\partial/\partial\varphi$ is the Cooper pair number operator, which is conjugate to the phase variable, φ, of the superconducting order parameter of the island. From Eq (9.6) (with $I = 0$), the potential energy is written $U = E_J \cos\varphi$, where we again defined a Josephson coupling energy, $E_J = I_0\Phi_0/2\pi$. The Hamiltonian of the system is then

$$H = K + U = 4E_C(\hat{N} - N_G)^2 + E_J \cos\varphi\,; \qquad (9.13)$$

this Hamiltonian is quantized via the commutation relation $\left[\hat{N}, \varphi\right] = i$.

The Double Junction Charge Qubit

The single junction device described above has the disadvantage that the only parameter that can conveniently be tuned is the gate voltage. We will show in Sect. 9.3.3 that, in spite of this limitation, it is still possible to perform arbitrary single qubit operations; however the procedures required turn out to be somewhat awkward and for this reason it is desirable to have a second, independent, parameter. As shown schematically in Fig. 9.12, this can be accomplished if we couple the island to a second Josephson junction that is connected to the first junction by a superconducting link such that a closed loop is formed; it is now assumed that a flux Φ_x is induced in this loop (by a second loop driven by an external current) such that a supercurrent passes through the two junctions (in addition to the island); this alters the Josephson critical current and with it the Josephson coupling energy and provides an *independently*

[1] Since the charging energy depends on the square of the gate potential, it is periodic in the Cooper pair number, and undergoes a splitting where $N_G = (2N+1)/2$, the E vs. N_G curves have the appearance of the E vs. k curves encountered in the theory of nearly free electrons in a one-dimensional crystal. In particular the point $N_G = 1/2$ corresponds to an electron at the first Brillouin zone point.

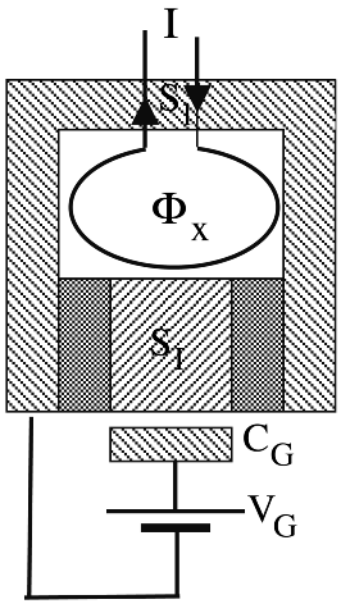

Fig. 9.12. A double junction qubit biased by a flux transformer

adjustable parameter. The device is variously called a hybrid device or Bloch transistor.

Assuming identical junctions one obtains the Hamiltonian as

$$\begin{aligned}\hat{H} &= E_C\left(\hat{N}-N_G\right)^2 + E_J(\cos\varphi_1+\cos\varphi_2)\\ &= E_C\left(\hat{N}-N_G\right)^2 + 2E_J\cos\varphi_x\cos\varphi\,;\end{aligned} \tag{9.14}$$

here $\varphi_x = \varphi_1 + \varphi_2 = \pi\Phi_x/\Phi_0$ and arises from the induced d.c. current flowing through the two junctions while $\varphi = \varphi_1 - \varphi_2$ where φ_1 and φ_2 are the phase shifts across the first and second junction respectively. The second term now acts as an *effective* Josephson coupling energy the strength of which can be tuned through the current I. Writing $2E_J^{\text{eff}} = 2E_J\cos(\theta/2)$ our Hamiltonian becomes

$$\hat{H} = E_C\left(\hat{N}-N_G\right)^2 + 2E_J^{\text{eff}}\cos\varphi \tag{9.15}$$

with

$$N_G = N_G(V_G)$$

and

$$E_J^{\text{eff}} = E_J^{\text{eff}}(\Phi_x)\,.$$

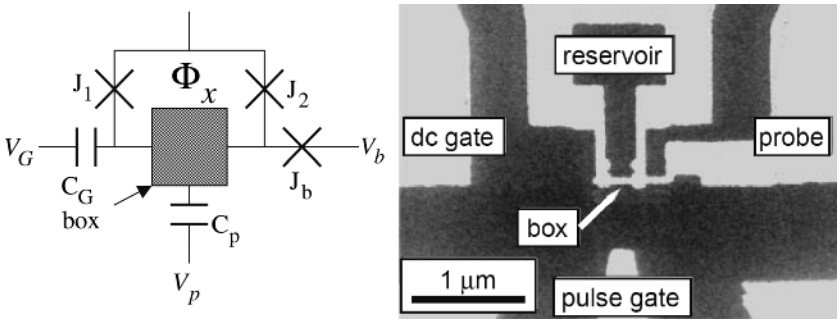

Fig. 9.13. Single-Cooper-pair box with a probe junction. *Left*: Circuit diagram of the device. The C's represent the capacitance of each element and the V's are voltages that can be applied to each electrode. *Right*: Micrograph of the sample; light areas are electrodes. The electrodes were fabricated by electron-beam lithography and shadow evaporation of Al on a SiN_x insulating layer (400 nm thick) above a gold ground plane (100 nm thick) on the oxidized Si substrate. The "box" electrode is a 700 × 50 × 15 nm Al strip containing $\sim 10^8$ conduction electrons. The reservoir electrode was evaporated after a slight oxidation of the surface of the box so that the overlapping area becomes two parallel low-resistance junctions ($\sim$ 10 kΩ in total) with Josephson energy E_J which can be tuned by a magnetic flux Φ penetrating through the loop. Before the evaporation of the probe electrode the box is further oxidized to create a highly resistive probe junction (R_b < 30 MΩ). Two gate electrodes (d.c. and pulse) are capacitively coupled to the box electrode. The sample was placed in a shielded copper case at the base temperature (T < 30 mK; k_BT < 3 μeV) of a dilution refrigerator. The single-electron charging energy of the box electrode $E_C = e^2/2C_I$ was 117 ± 3 meV, where C_I is the total capacitance of the box electrode. The superconducting gap energy Δ was 230 ± 10 μeV

The Double Junction Charge Qubit with a Readout Junction

By including a third or "probe" junction, readout can be facilitated [26]. Such a device is shown in Fig. 9.13. The right side is an electron micrograph of the device itself while the left side shows a schematic diagram. As with the simplified double junction device, it involves a small superconducting island on which N excess Cooper-pairs (relative to some neutral reference state) can reside. The island is again electrostatically coupled through a capacitance C_G to a control gate G, that biases the charge on the island; however an additional capacitance, C_p, is also included to allow *control pulses* to be inserted. As noted, the inclusion of a third junction allows read out; this is accomplished by biasing the device far from the degeneracy point causing the superposition state to collapse.

Figure 9.14 shows a similar device that the original authors [27] refer to as a *quantronium circuit*. Activating the bias current I_b, drives the qubit away from its optimal working point and is again used to readout the quantum state. The circuit was fabricated by depositing aluminum through a suspended mask that was in turn patterned by e-beam lithography. It consists of a superconducting loop interrupted by two small Josephson tunnel junctions, each with capacitance C_J (having a low series capacitance) and Josephson energy E_J, a superconducting island with capacitance C_I, and by a large Josephson junction E_{J0} with energy $E_{J0} \cong 20E_J$. The island is again charge-

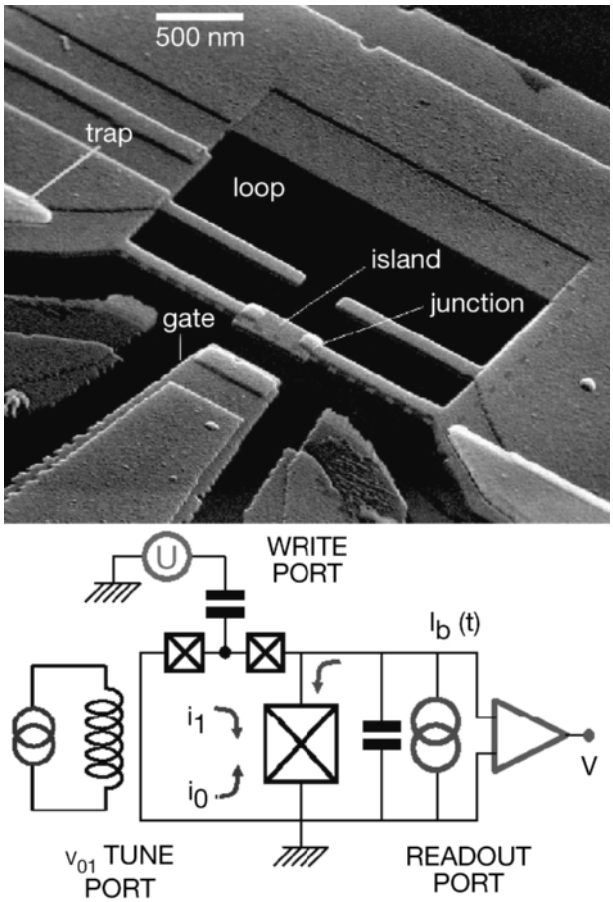

Fig. 9.14. *Top*: scanning electron micrograph of the circuit. *Bottom*: schematic diagram showing the tuning, preparation and readout blocks

biased by a voltage source V_G through a gate capacitance C_G; it *is* flux-biased by a loop that generates clockwise or counter-clock wise currents through the junctions.

Experimental studies have been performed by several groups with aluminum tunnel junctions with dimensions below 100 nm [4,28]. The superposition of charge states in circuits in the charging regime has been demonstrated [29–31] and is in quantitative agreement with theory [32,33]. The Heisenberg uncertainty principle has been demonstrated when $E_J \approx E_C$. [34] When $E_J > E_C$ topological excitations involving vortices exist (which we do not discuss) and quantum mechanical interference of these quantities has been observed [34]. Unfortunately circuits of the first type in the charging regime are sensitive to fluctuating "off-set charges" that are present in the substrate [35,36]. These random offset charges make the design of a controllable array of quantum circuits difficult and introduce a strong source of decoherence.

The Charge-State Basis

In a bulk superconductor one usually characterizes the macroscopic quantum state by the Ginzburg-Landau phase and regards the Cooper pair number as a fluctuating quantity. However when the island charging energy significantly exceeds the Josephson coupling energy, $E_c \gg E_J$, states $|N\rangle$ numbered by the excess number of Cooper pairs N on the island form a good basis. In this basis the Hamiltonian (9.13) is written

$$\hat{H} = \sum_N \left\{ 4E_C \left(\hat{N} - N_G\right)^2 |N\rangle \langle N| - \frac{1}{2} E_J \left[|N\rangle \langle N+1| + |N+1\rangle \langle N| \right] \right\} . \tag{9.16}$$

When N differs significantly from N_G the energy levels are dominated by the charging part of the Hamiltonian. However, when N_G is approximately a half-integer, the charging energies of two adjacent states that differ by a Cooper pair are close to each other (e.g., at $V_G = V_{\rm deg} \equiv e/C_G$), and the Josephson tunneling strongly mixes them (see Fig. 9.11). If we focus on voltages near such a degeneracy point, *only two* charge states (say $N = 0$ and $N = 1$) play a role; all other charge states have a much higher energy and can be ignored. In this case the Cooper box Hamiltonian (9.16) reduces to a *two-state quantum system* (a qubit) with a Hamiltonian that in spin-1/2 notation can be written as

$$\hat{H} = -\frac{1}{2} B_z \hat{\sigma}_z - \frac{1}{2} B_x \hat{\sigma}_x . \tag{9.17}$$

The charge states $N = 0$ and $N = 1$ associated with the diagonal operator $\hat{\sigma}_z$ are given by

$$|\uparrow\rangle = \begin{pmatrix} 1 \\ 0 \end{pmatrix}; |\downarrow\rangle = \begin{pmatrix} 0 \\ 1 \end{pmatrix} \tag{9.18}$$

respectively and the effective magnetic field B_z corresponds to the charging energy, which is controlled by the gate voltage and is given by

$$B_z = \delta E_{ch} \equiv 4E_c \left(1 - 2N_G\right) . \tag{9.19}$$

On the other hand, $B_x \equiv E_J$, associated with the off diagonal operator $\hat{\sigma}_x$, couples states differing by one Cooper pair.

We now rewrite the Hamiltonian (9.17) as

$$\hat{H} = -\Delta E\left(\kappa\right) \left(\cos\kappa \hat{\sigma}_z + \sin\kappa \hat{\sigma}_x\right)/2 , \tag{9.20}$$

where the *mixing angle*

$$\kappa \equiv \tan^{-1}\left(B_x/B_z\right) \tag{9.21}$$

determines the direction of the effective magnetic field in the x–z plane. The eigenvalues of (9.20) are given by

$$\Delta E\left(\kappa\right) = \sqrt{B_x^2 + B_z^2} = E_J/\sin\kappa \tag{9.22}$$

and the eigenstates, $|0\rangle$ and $|1\rangle$, by

$$|0\rangle = \cos\frac{\kappa}{2}|\uparrow\rangle + \sin\frac{\kappa}{2}|\downarrow\rangle , \tag{9.23a}$$

$$|1\rangle = -\sin\frac{\kappa}{2}|\uparrow\rangle + \cos\frac{\kappa}{2}|\downarrow\rangle . \tag{9.23b}$$

The point where the two charge states are degenerate corresponds to $B_z = 0$, or equivalently $\kappa = \pi/2$; here $\Delta E = E_J$. We can now rewrite the Hamiltonian in diagonal form as

$$\hat{H} = -\frac{1}{2}\Delta E\left(\kappa\right)\hat{\rho}_z , \tag{9.24}$$

where we have introduce a second set of Pauli matrices, $\hat{\rho}$, that operate in the $|0\rangle, |1\rangle$ basis, while retaining the $\hat{\sigma}$ operators for the charge-state basis, $|\uparrow\rangle, |\downarrow\rangle$.

The Hamiltonian (9.24) is similar to the ideal single-qubit model. Ideally the bias energy (the effective magnetic field in the z direction) and the tunneling amplitude (the field in the x direction) are controllable, a property of the hybrid devices discussed above. As noted above, it turns out that we can perform all qubit operations using only a single parameter, the bias energy (through the gate voltage); this situation will be considered in Sect. 9.3.3. Operations that include tuning the tunneling amplitude, which fixes the Josephson energy, will be considered in Sect. 9.3.3.

9.2.5 Flux Qubits

In circuits of the second type identified in Sect. 9.2.1 ($L_s \gg L_J$), the quantum variables can be related to the flux in the loops and their time derivatives.

The circuits involve a superconducting ring that is interrupted by one or more Josephson junctions in which a persistent current flows with its associated magnetic flux. The flux-based qubits emerge from the following ideas. We recall that flux is quantized within a superconducting loop; i.e.,

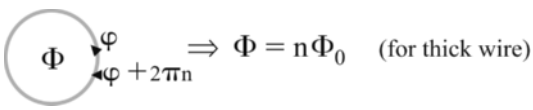

If we now insert a Josephson junction in the loop (see Fig. 9.15) the phase difference across the junction will be related to the flux Φ within the loop, which in units of the flux quantum, $\Phi_0 = h/2e$, is written

$$\Phi = \Phi_0 \left(n - \frac{\varphi}{2\pi} \right) , \tag{9.25}$$

where n is an integer number and $\varphi = 2\pi(\Phi/\Phi_0)$. When the system is biased by an externally applied flux Φ_x, the Hamiltonian (which includes the Josephson, charging, and magnetic contributions to the energy) is written as

$$H = E_C + E_J + \frac{1}{2} LI^2 , \tag{9.26}$$

where

$$E_C = \frac{Q^2}{2C_J}; \qquad E_J = -E_0^J \cos\left(2\pi \frac{\Phi}{\Phi_0} \right); \qquad \frac{1}{2} LI^2 = \frac{(\Phi - \Phi_x)^2}{2L}; \tag{9.27}$$

here L is the self-inductance of the loop and C_J is the capacitance of the junction. In quantizing (9.26) we interpret the charge as an operator $Q = -i\hbar\partial/\partial\Phi$ that is canonically conjugate to the flux Φ.

If the self-inductance is large, such that the parameter $\beta_L = E_0^J / \left(\Phi_0^2 / 4\pi^2 L \right)$ is larger than 1, and the externally applied flux Φ_x is close to $\Phi_0/2$, the second and third terms in the Hamiltonian (9.26),

$$U = U_0 \left[\frac{1}{2} \left(\varphi - \varphi_x \right)^2 - \beta_L \cos\left(\varphi \right) \right] , \tag{9.28}$$

form a double-well potential (see Fig. 9.16); here $\varphi = 2\pi\Phi/\Phi_0, \varphi_x \equiv 2\pi(\Phi_x/\Phi_0)$, and $U_0 = \Phi_0^2/(4\pi^2 L)$. At low temperatures only the lowest states in the two wells contribute.

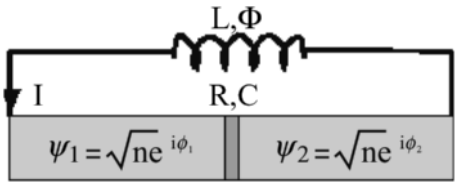

Fig. 9.15. A Josephson junction shunted by an external inductor

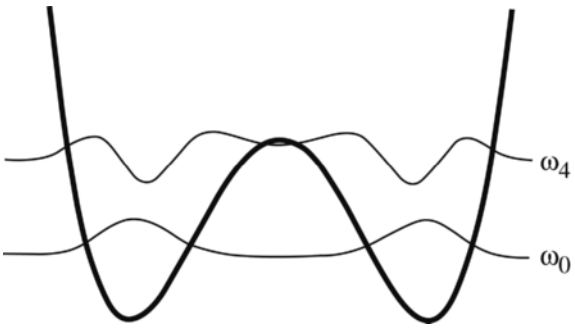

Fig. 9.16. A typical two-level system

Analogous to Eq. (9.17) for the charge qubit, the reduced Hamiltonian of this effective two-state system can again be written in the form

$$\hat{H} = -B_z\hat{\sigma}_z/2 - B_x\hat{\sigma}_x/2\,.$$

The diagonal term B_z plays the role of a bias; when $\beta_L - 1 \ll 1$ we can expand the cosine and the asymmetry of the double-well potential can then be represented by a field

$$B_z\left(\varphi_x\right) = 4\pi\sqrt{6\left(\beta_L - 1\right)}E_J\left(\varphi_x - 1/2\right)\,. \qquad (9.29)$$

B_z can be tuned through the applied flux Φ_x via an applied current I_x. The off-diagonal term B_x describes the tunneling amplitude between the wells, which depends on the height of the barrier and thus on the Josephson energy E_J; this energy can be controlled if the junction is *replaced by a dc SQUID with the flux* $\tilde{\Phi}_x$ introduced as another control variable [8]. With these two external control parameters the elementary single-bit operations, i.e., z and x rotations, can be performed, which are equivalent to the manipulations described in the previous section for charge qubits.

Flux qubit operations can be performed either by abrupt switching of the external fluxes Φ_x and $\tilde{\Phi}_x$ for a finite time, or with the use of r.f. fields and resonant pulses. Such a devices constitutes the r.f. SQUID used in the experiments [37–40]. To permit coherent manipulations, the parameter β_L in Eq. (9.29) should be chosen larger than unity (so that two minima with well-defined levels appear), but not so large that the resulting barrier height between the minima, ΔU, overly suppresses the tunneling; these energetics are shown in Fig. 9.16.

The r.f. SQUID described above, which mimics an asymmetric quantum well (shown in Fig. 9.17), was discussed in the mid 1980's as a realization of a two-state quantum system. Some features of macroscopic quantum behavior were demonstrated, such as macroscopic quantum tunneling of the flux, resonant tunneling, and level quantization [41–44]. However, only very recently has the level repulsion near a degeneracy point been demonstrated [45,46]. For the r.f. SQUID, thermal activation of macroscopic quantum states [47] has been observed as well

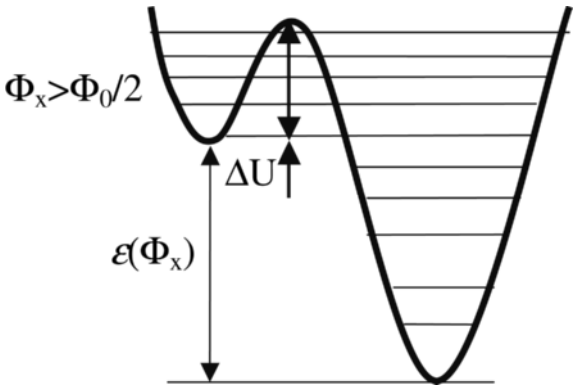

Fig. 9.17. The asymmetric quantum well; biasing is achieved by a flux Φ_x. The level structure is probed using macroscopic resonant tunneling

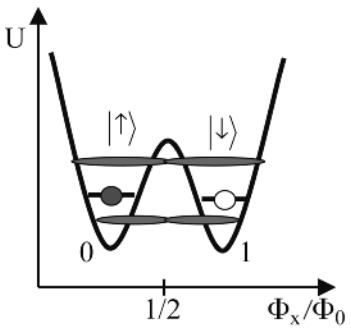

Fig. 9.18. The SQUID level splitting versus the magnetic flux Φ_x in the double-well potential U. The two states have circulating currents of opposite sign

as macroscopic quantum tunneling between states shown schematically in Fig. 9.18 [48].

Caldeira and Leggett [49] proposed these systems in the mid 1980s as test objects to study various quantum-mechanical effects, including macroscopic quantum tunneling of the phase (or flux) as well as resonant tunneling. Both the effects have been observed in several experiments [50–53]. An advantage of such devices is that the two persistent current states can be externally distinguished, since they involve circulating currents of *opposite sign* (see Fig. 9.18). This leads to alternative qubit design that exploits circuits of the first type (with aluminum), but which utilizes states associated with circulating currents having opposite sign (as in circuits of the second type). These circulating current

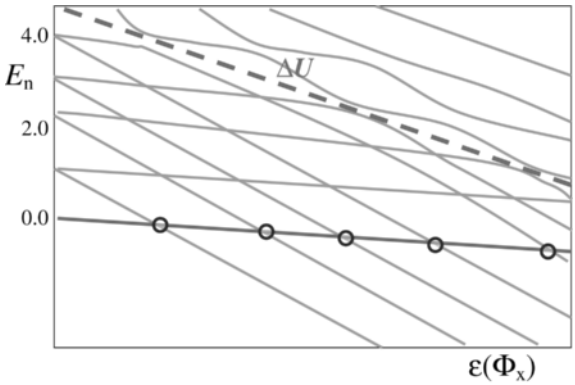

Fig. 9.19. The energy level positions versus the tilt of the double well potential in a SQUID-type device. The avoided level crossing is indicated by the *dashed line*

states typically create a magnetic flux $\sim 10^{-3}\Phi_0$ so-called "persistent current (PC) states". These states obey all of the five requirements for a quantum bit: (1) they can readily be prepared in the ground state (at a sufficiently low temperature); (2) they can be precisely manipulated with magnetic fields; (3) two qubits can be coupled inductively, and that coupling can be switched on and off; (4) the flux associated with the PC states can be measured using a SQUID-type detector; and (5), the states can be made insensitive to background charges and effectively decoupled from their electrostatic environment (in contrast with charge quantum states in Josephson circuits); the magnetic coupling to the environment can also be effectively suppressed.

Another important quantum effect has been reported recently: The groups at Stony Brook [54] and Delft [55] have experimentally observed the *avoided level crossing* due to coherent tunneling of the flux in a double-well potential. In principle, all other manipulations discussed in the previous section should be possible with Josephson flux devices as well. The group at Stony Brook probed, spectroscopically, the superposition of excited states in different wells. The experimental results are shown in Fig. 9.19 for an r.f. SQUID with a self-inductance $L = 240$ pH and $\beta_L = 2.33$. In the experiment a substantial separation of the minima of the double-well potential (of order Φ_0) and a high inter-well barrier made the tunnel coupling between the lowest states in the wells negligible. However, both wells contain a set of higher localized levels (under suitable conditions one state in each well) with relative energies that are also controlled by Φ_x and $\tilde{\Phi}_x$. Because they were closer to the top of the barrier, these states mixed more strongly and formed eigenstates, which were superpositions of localized flux states from different wells. External microwave radiation was then used to pump the system from a well-localized lowest state in one well to one of these eigenstates. The energy spectrum of these levels was studied for different biases Φ_x, $\tilde{\Phi}_x$, and the properties of the model associated with Eq. (9.28) were confirmed. In particular, the level splitting at the degeneracy point indicated a superposition of distinct quantum states. They differed in a macroscopic way: the authors estimated that the parameters associated with the two superimposed flux states differed by a flux $\Phi_0/4$, a current of 2–3 mA, and a magnetic moment of $10^{10}\mu_B$.

9.3 Qubit Dynamics

In this section we begin by discussing the manipulation of single qubit devices by an external time dependent field. In realistic mesoscopic systems, there are usually several discrete energy levels (e.g. the three levels utilized in a phase qubit). However a qubit utilizes only two of these levels and therefore care must be taken to isolate these levels from the remaining levels. Assuming for the moment that this is the case, we first review the quantum mechanics associated with transitions within a two-level system, which is fundamental to the operation of all qubits.

9.3.1 Transitions Within Two-Level Systems; the Rabi Frequency

Assume we are given a system with discrete levels E_n and states $\Phi(q, t)$ (where q denotes all spatial coordinates) that is perturbed by an external time-dependent field, $\hat{V}(t)$. We seek an approximate solution to the time-dependent Schrödinger equation,

$$i\hbar\frac{\partial\Psi}{\partial t} = \left(\hat{H}_0 + \hat{V}(t)\right)\Psi\,, \tag{9.30}$$